

Determination of N^* amplitudes from associated strangeness production in p+p collisions

R. Münzer,^{1,2,*} L. Fabbietti,^{1,2,†} E. Epple,³ S. Lu,² P. Klose,² F. Hauenstein,⁴ N. Herrmann,⁵ D. Grzonka,^{4,6,7} Y. Leifels,⁸ M. Maggiora,⁹ D. Pleiner,² B. Ramstein,¹⁰ J. Ritman,^{4,6,7} E. Roderburg,⁴ P. Salabura,¹¹ A. Sarantsev,¹² Z. Basrak,¹³ P. Buehler,¹⁴ M. Cargnelli,¹⁴ R. Čaplar,¹³ H. Clement,^{15,16} O. Czerwiakowa,¹⁷ I. Deppner,⁵ M. Dželalija,¹⁸ W. Eyrich,¹⁹ Z. Fodor,²⁰ P. Gasik,^{1,2} I. Gašparić,¹³ A. Gillitzer,^{4,6,7} Y. Grishkin,²¹ O.N. Hartmann,⁸ K.D. Hildenbrand,⁸ B. Hong,²² T.I. Kang,^{8,22} J. Kecskemeti,²⁰ Y.J. Kim,⁸ M. Kirejczyk,¹⁷ M. Kiš,⁸ P. Koczon,⁸ R. Kotte,²³ A. Lebedev,²¹ A. Le Fèvre,⁸ J.L. Liu,²⁴ V. Manko,²⁵ J. Marton,¹⁴ T. Matulewicz,¹⁷ K. Piasecki,¹⁷ F. Rami,²⁶ A. Reischl,⁵ M.S. Ryu,²² P. Schmidt,¹⁴ Z. Seres,²⁰ B. Sikora,¹⁷ K.S. Sim,²² K. Siwek-Wilczyńska,¹⁷ V. Smolyankin,²¹ K. Suzuki,¹⁴ Z. Tyimiński,⁵ P. Wagner,²⁶ I. Weber,¹⁸ E. Widmann,¹⁴ K. Wiśniewski,¹⁷ Z.G. Xiao,²⁷ T. Yamasaki,^{28,29} I. Yushmanov,²⁵ P. Wintz,⁴ Y. Zhang,³⁰ A. Zhilin,²¹ V. Zinyuk,⁵ and J. Zmeskal¹⁴

¹Excellence Cluster Universe, Technische Universität München, Boltzmannstr. 2, D-85748, Germany

²Physik Department E62, Technische Universität München, 85748 Garching, Germany

³Yale University, New Haven, Connecticut, United States

⁴Institut für Kernphysik, Forschungszentrum Jülich, 52428 Jülich, Germany

⁵Physikalisches Institut der Universität Heidelberg, Heidelberg, Germany

⁶Jülich Aachen Research Alliance, Forces and Matter Experiments (JARA-FAME)

⁷Experimentalphysik I, Ruhr-Universität Bochum, 44780 Bochum, Germany

⁸GSI Helmholtzzentrum für Schwerionenforschung GmbH, 64291 Darmstadt, Germany

⁹Istituto Nazionale di Fisica Nucleare (INFN) - Sezione di Torino, 10125 Torino, Italy

¹⁰Institut de Physique Nucléaire, CNRS/IN2P3 - Univ. Paris Sud, F-91406 Orsay Cedex, France

¹¹Smoluchowski Institute of Physics, Jagiellonian University of Cracow, 30-059 Kraków, Poland

¹²Petersburg Nuclear Physics Institute, Gatchina, Russia

¹³Ruder Bošković Institute, Zagreb, Croatia

¹⁴Stefan-Meyer-Institut für subatomare Physik, Österreichische Akademie der Wissenschaften, Wien, Austria

¹⁵Physikalisches Institut der Universität Tübingen,

Auf der Morgenstelle 14, 72076 Tübingen, Germany

¹⁶Kepler Center for Astro and Particle Physics, University of Tübingen,

Auf der Morgenstelle 14, 72076 Tübingen, Germany

¹⁷Institute of Experimental Physics, Faculty of Physics, University of Warsaw, Warsaw, Poland

¹⁸Faculty of Science, University of Split, Split, Croatia

¹⁹Friedrich-Alexander-Universität Erlangen-Nürnberg, 91058 Erlangen, Germany

²⁰Wigner RCP, RMKI, Budapest, Hungary

²¹Institute for Theoretical and Experimental Physics, Moscow, Russia

²²Korea University, Seoul, Korea

²³Institut für Strahlenphysik, Helmholtz-Zentrum Dresden-Rossendorf, Dresden, Germany

²⁴Harbin Institute of Technology, Harbin, China

²⁵National Research Centre 'Kurchatov Institute', Moscow, Russia

²⁶Institut Pluridisciplinaire Hubert Curien and Université de Strasbourg, Strasbourg, France

²⁷Department of Physics, Tsinghua University, Beijing, China

²⁸Department of Physics, The University of Tokyo, Tokyo, 113-0033

²⁹RIKEN Nishina Center, RIKEN, Wako, 351-0198, Japan

³⁰Institute of Modern Physics, Chinese Academy of Sciences, Lanzhou, China

We present the first determination of the energy-dependent amplitudes of N^* resonances extracted from their decay in $K\Lambda$ pairs in $p+p \rightarrow pK^+\Lambda$ reactions. A combined Partial Wave Analysis of seven data samples with exclusively reconstructed $p+p \rightarrow pK^+\Lambda$ events measured by the COSY-TOF, DISTO, FOPI and HADES Collaborations in fixed target experiments at kinetic energies between 2.14 to 3.5 GeV is used to determine the amplitude of the resonant and non-resonant contributions into the associated strangeness final state. The contribution of seven N^* resonances with masses between 1650 MeV/c² and 1900 MeV/c² for an excess energy between 0 and 600 MeV has been considered. The Σ -p cusp and final state interactions for the p - Λ channel are also included as coherent contributions in the PWA. The N^* contribution is found to be dominant with respect to the phase space emission of the $pK^+\Lambda$ final state at all energies demonstrating the important role played by both N^* and interference effects in hadron-hadron collisions.

Keywords: partial wave analysis, resonance, hadrons, strangeness, scattering length, hyperon-nucleon interaction

INTRODUCTION

The production of strange hadrons within nuclear matter is a key ingredient in the understanding of the in-

nermost structure of neutron stars (NS). Indeed, several

theoretical models predict that the production of strange hadrons is energetically favourable already at moderate densities of neutron-rich matter [1, 2] and hence neutron stars with strange hadrons could appear. On the other hand, the appearance of strange hadrons softens the equation of state of NS excluding the existence of massive NS unless a strong repulsive interaction is assumed for the Λ NN system [3]. Since NS with two solar masses have already been measured with high precision [4, 5], this situation translates into a puzzle that can be solved only studying hyperons and kaons production in hadron-hadron collisions. The best environment to carry out this kind of studies is provided by hadron-hadron collisions at few GeV kinetic energies because at these energies large baryonic densities, similar to those within NS, can be created. On the other hand the reaction dynamics at these energies is dominated by hadronic resonances, that need then to be quantitatively understood [6–13].

For final states containing pions and nucleons produced in elementary reactions, partial wave analysis (PWA) was already employed to correctly take into account interferences among resonances and determine the amplitude of the contributing waves [14–17]. For the contribution of resonances to final states with open strangeness the reaction $N^* \rightarrow K + \Lambda$ was first studied by analyzing the Dalitz plot for the reaction $p + p \rightarrow p + K^+ + \Lambda$ up to kinetic energies of $T = 2.5$ GeV, but without accounting for interference effects [13]. The HADES collaboration was the first to employ a PWA for the search for the kaonic bound state ppK^- [18, 19] in the reaction $p + p \rightarrow p + K^+ + \Lambda$ at a beam kinetic energy of 3.5 GeV. In this reaction it was found that N^* contribute to the measured final state and influence the background for the kaonic bound state [20, 21]. No evidence for the existence of ppK^- bound states could be found and upper limits for the production of such states of the order of a few μb were extracted. To get a consistent description of the open strangeness production, we further improve this method and develop a framework that allows for the simultaneous analysis of seven different data sets measured in the $p + p \rightarrow p + K^+ + \Lambda$ reaction by the COSY-TOF, HADES, DISTO and FOPI experiments in fixed target experiments at kinetic energies in the laboratory frame varying from 2.14 to 3.5 GeV [20, 22–27]. This is the very first joint PWA analysis of different data sets for this reaction. This way, the energy-dependent amplitude of seven different contributing N^* resonances decaying into the Λ - K^+ channel and for non-resonant $pK^+\Lambda$ final states could be extracted for the first time.

A second interesting aspect is the study of the p - Λ interaction. This interaction was previously investigated primarily by means of scattering experiments [28–30]. The reaction $p + p \rightarrow p + K^+ + \Lambda$ offers the possibility to study the final state interaction of the p - Λ pair as an alternative to scattering experiments [27, 30–32]. Since so

far the resonances were not treated in a coherent way, a precise determination of their contributions and of the scattering lengths and effective ranges was challenging. The combined PWA presented in this work offers the unique possibility to study the interplay between the N^* coupling to the Λ - K^+ channel and the p - Λ final state interaction.

DATA SAMPLES AND COMBINED ANALYSIS

The experimental data were measured by the COSY-TOF, DISTO, FOPI and HADES Collaborations. Table I provides an overview of the data sets used for the combined PWA, their beam energy and number of events. Together with each experimental data set, simulations of the $pK^+\Lambda$ production according to phase space kinematics, filtered through the detector simulation and analysed as the experimental data are used for the PWA. The details about the reconstruction of the exclusive $pK^+\Lambda$ final state, achieved resolution, efficiency, and purity are explained in the already published works by the different collaborations [20, 22–27]. The two HADES data samples at the same kinetic energy correspond to two different reconstruction analyses including or excluding the forward spectrometer [20]. These data sets are complementary and do not share any reconstructed events because of the exclusive selection of the final state.

The goal of this PWA is to employ the seven data samples in a combined analysis and extract the amplitudes of the different waves, characterised by their quantum numbers, leading to given final states. We use the Bonn-Gatchina PWA (BG-PWA) framework [15, 16] to fit event-by-event the measured 4-momenta for the exclusive final state $p + p \rightarrow p + K^+ + \Lambda$ weighted with the coherent superposition of specific participating waves. The best choice for the waves used in the PWA is determined by comparing the experimental data to the PWA output event-by-event in terms of a log-likelihood parameter. In the specific case of the COSY-TOF data sample, only the region of phase space within $|\cos\theta_p^{\text{CM}}| < 0.7$, where θ_p^{CM} is the proton angle in the p - p center of mass system, was considered because of the poor description of the trigger efficiency in the simulation for the excluded region. For the DISTO data samples the region corresponding to $\cos\theta_p^{\text{CM}} > 0.95$ was excluded from the fit to minimize the bias introduced by the digitization of the scintillation-fiber sub detector used for tracking close to the target region. These cuts were also added in the simulations used in the PWA analysis procedure.

This PWA allows to decompose the baryon-baryon scattering amplitude into separate sub-processes characterized by different intermediate states. Within the BG-PWA framework this is achieved by fitting event-by-event the experimental 4-vectors for a given reaction measured within the acceptance of the spectrometer with a coher-

TABLE I. List of available number of events for the reaction $p+p \rightarrow p+K^++\Lambda$ measured by the COSY-TOF, DISTO, FOPI and HADES Collaborations. The kinetic beam energy, the total cross section and the reduced χ^2 values resulting from different PWA analyses are shown (see text for details).

experiment	T (GeV)	Events/ndf	σ_{tot} [μ b]	χ^2/ndf (single)	χ^2/ndf (combined)
DISTO [22, 23]	2.14	121000 / 644	19.0 ± 3.3	0.52	1.52
COSY-TOF [25, 27]	2.16	43662 / 712	19.7 ± 3.5	1.69	0.44
DISTO [22, 23]	2.5	304000 / 766	30.5 ± 5.7	2.85	2.56
DISTO [22–24]	2.85	424000 / 555	38.7 ± 7.9	7.68	3.55
FOPI [26]	3.1	903 / 226	43.1 ± 9.3	1.21	0.91
HADES [20]	3.50	13155 / 528	48.0 ± 11.5	1.12	2.14
HADES [20]	3.50	8155 / 534	48.0 ± 11.5	1.38	1.86

TABLE II. N^* resonances included in the PWA written in the spectroscopic notation with the corresponding masses, widths and branching ratios in the $K\Lambda$ final states [33, 34].

N^*	J^P	Mass ($\frac{\text{GeV}}{c^2}$)	Width ($\frac{\text{GeV}}{c^2}$)	$\Gamma_{K\Lambda}/\Gamma_{tot}$ (%)
1650	$\frac{1}{2}^-$ [33]	1.655	0.14	7 ± 4
1710	$\frac{1}{2}^+$ [33]	1.710	0.23	15 ± 10
1720	$\frac{3}{2}^+$ [33]	1.720	0.25	4 ± 1
1875	$\frac{3}{2}^-$	1.875	0.20 [33]	4 ± 2 [34]
1880	$\frac{1}{2}^+$	1.870	0.24 [34]	2 ± 1 [34]
1895	$\frac{1}{2}^-$	1.895	0.09 [34]	18 ± 5 [34]
1900	$\frac{3}{2}^+$	1.900	0.26 [34]	11 ± 9 [33]

ent superposition of the participating waves. This coherent cocktail of contributing waves is weighted with the full scale phase space simulations of the considered final state that accounts for the geometrical acceptance and reconstruction efficiency of the spectrometer.

Within the BG-PWA, the production cross section of a three particle final state with single particle four-momenta $q_{1,2,3}$ is parametrized as [15]:

$$d\sigma = \frac{(2\pi)^4 |A|^2}{4|\vec{k}|\sqrt{s}} d\Phi_3(P, q_1, q_2, q_3), \quad (1)$$

wherein P is the total four-vector, \vec{k} is the beam momentum, \sqrt{s} the center of mass energy of the reaction, $d\Phi_3$ is the infinitesimal phase-space volume of the final state and A is the total transition amplitude of the considered reaction. Both initial and final states can be seen as a superposition of eigenstates with various angular momentum and A is the sum over all the transition amplitudes A_{tr}^α between these eigenstates [35]:

$$A = \sum_{\alpha} A_{tr}^\alpha(s) Q_{\mu_1 \dots \mu_j}^{\text{in}}(S, L, J) A_{2b}(i, S_2, L_2, J_2) Q_{\mu_1 \dots \mu_j}^{\text{fin}}(i, S_2, L_2, J_2, S', L', J). \quad (2)$$

The index α runs over all the amplitudes contributing to the transition from the initial to the final state. The factors $Q_{\mu_1 \dots \mu_j}^{\text{in}}(S, L, J)$ and $Q_{\mu_1 \dots \mu_j}^{\text{fin}}(i, S_2, L_2, J_2, S', L', J)$ are the spin-momentum operators of the initial and final states respectively and the indexes μ_j refer to the rank of the total angular momentum J in the spin-momentum operators Q . The index i refers to the two-particle subsystem considered in the final state.

The dependency of the amplitudes $A_{tr}^\alpha(s)$ upon the centre of mass energy is given by:

$$A_{tr}^\alpha(s) = (a_1^\alpha + a_3^\alpha \sqrt{s}) \exp(i a_2^\alpha). \quad (3)$$

The real parameters a_1^α , a_2^α and a_3^α are determined by the fit to the experimental data.

The parametrization of the factor A_{2b} depends on the final state. For the production of a N^* resonance, the final state is treated as a two-body system composed of a proton and the N^* . In this case the quantum numbers S_2, L_2, J_2 refers to the N^* , while the S', L', J represent the quantum numbers of the N^* -proton system. Non resonant $pK^+\Lambda$ final states are also treated as a two particle system composed of a $p\Lambda$ "particle" and a K^+ . In this case S_2, L_2, J_2 are the spin, angular and total angular momentum of the $p\Lambda$ 'particle' while S', L', J are the quantum numbers of the $p\Lambda$ - K^+ system.

For the resonant case, the factor A_{2b} is parametrized with a relativistic Breit-Wigner formula [36].

$$A_{2b}^\beta = \frac{1}{(M^2 - s - i\Gamma M)}, \quad (4)$$

with M and Γ as the pole mass and width of the corresponding resonance. For the presented analysis, the N^* resonances listed in Table II have been considered with fixed masses and fixed widths taken from [33, 34].

To obtain an acceptable description of the experimental data it is necessary to include non-resonant partial wave amplitudes. We have included these amplitudes in a simple form which provides a correct behaviour near threshold. For the S-wave this form corresponds to the well

known Watson-Migdal parameterization. The resulting A_{2b} amplitude is

$$A_{2b}^\beta = \frac{\sqrt{s_i}}{1 - \frac{1}{2}r^\beta q^2 a_{p\Lambda}^\beta + iqa_{p\Lambda}^\beta q^{2L}/F(q, r^\beta, L)}, \quad (5)$$

where q is the p - Λ relative momentum, $a_{p-\Lambda}^\beta$ is the p - Λ -scattering length, r^β is the effective range of the p - Λ system and the index β denotes the quantum numbers combination.

$F(q, r, L)$ is the Blatt-Weisskopf factor used for the normalization, it is 1 for $L=0$ and the explicit form for other partial waves can be found in [15]. The values of the scattering length and effective range can be set as free parameters in the PWA fit and hence be extracted within this analysis. This coherent approach differs from the analysis techniques usually employed for the extraction of scattering parameters [37] and should be considered as complementary.

Another intermediate channel contributing to $pK^+\Lambda$ final state is the Σ - N cusp, which appears at or above the Σ - N threshold (2130 MeV/ c^2) [38]. The coupling between the Σ - N and Λ - N channels leads to an enhancement of the cross-section in the p - Λ final state in a mass range close to the above mentioned threshold. In order to include the cusp contribution in the BG-PWA framework, new transition waves must be added to Eq. 2. Since the cusp is located at the Σ - N threshold, the Σ and N must be in a relative S-wave state, which means that the spin-parity of the Σ - N system is either $J^P = 0^+$ or 1^+ [38]. The resulting p - Λ system then may appear in an S-wave state in case of $J^P = 0^+$ or in an s- or d-wave state in case of $J^P = 1^+$. This has also been confirmed by an analysis of the Σ - N cusp carried out by the COSY-TOF collaboration [38]. Additionally, since the cusp is a resonance structure in analogy to the N^* , the Breit-Wigner parametrization is used for A_{2b} (Eq. 4) where the mass and width are varied within 2.1 – 2.16 GeV and 0.01 – 0.03 GeV/ c^2 , respectively in the PWA fit. This first attempt can be also replaced by a more sophisticated parametrization of the cusp contribution like a Flatté' function, but this is beyond the scope of this investigation. Indeed the cusp contribution has a negligible effect on the determination of the N^* contributions.

RESULTS

First, the PWA was performed individually for the different data samples to determine the correct start values of the parameters for the global fit. The total number of available degrees of freedom for each data set is listed in Table I. The total number of free parameters in the PWA fit containing all accessible N^* is equal to 345 ± 17 , the error refers to the systematic variation of the contribut-

ing N^* considered in the global fit. The best solution of the PWA fit corresponds to the minimum of the log-likelihood obtained by fitting the experimental data with the PWA event-by-event.

A comparison of the three missing mass spectra and CM, Gottfried-Jackson and Helicity angle distributions (for the definition of these variables see [11]) obtained from the experimental data and from the single PWA fits was carried out and the corresponding reduced χ^2 values are listed in Table I. Only the statistical error of the experimental data has been considered to evaluate the χ^2 of the single PWA fits. As a second step, a simultaneous PWA of three data samples was carried out. This intermediate step allowed to determine the starting values for the global fit. The HADES, FOPI and DISTO ($T = 2.5$ GeV) samples were selected to account for both the contributions from the Σ - N cusp and from higher mass resonances. After finding a solution that described the three data samples, further data samples were added stepwise. The starting values of each new PWA fit were taken from the results of the previous fit step. The systematic error of the experimental samples have not been considered in the fit since the latter were not available for all the data sets. To account for possible systematic variations of the kinematic distributions we have considered all permutations for the exclusion of one or more N^* resonances from the list in Table II in the PWA fit. The five best solutions in terms of log-likelihood obtained from this systematic variation of the PWA fits were considered to extract the final results and the PWA systematic errors. As far as the resonances are concerned, considering the list of seven resonances in Table II, the five best solutions correspond to the following combinations: 1) all seven N^* included, 2) $N^*(1720)$ excluded, 3) $N^*(1875)$ excluded, 4) $N^*(1900)$ excluded and, 5) $N^*(1900)$ and $N^*(1875)$ excluded. The reduced χ^2 values for the combined PWA listed in Table I were obtained by comparing the experimental data in the mass and angle variables with the average values of the five best PWA solutions, taking as errors the statistical errors of the experimental data and the standard deviation of the five solutions for each bin. By adding additional solutions the χ^2 did not improve. This justifies the choice of the five best solutions. A more refined treatment of systematic uncertainties is current under development.

Figure 1 shows the missing mass distributions (MM) for the three final state particles p , Λ and K^+ for COSY-TOF at 2.16 GeV (blue symbols), DISTO at 2.85 GeV (green symbols) and HADES at 3.5 GeV (red symbols) data samples measured within their respective acceptances and arbitrarily normalized. The signature of the Σ - N cusp is visible in the COSY-TOF and DISTO MM_{K^+} distribution around 2.13 GeV/ c^2 . The errors of the experimental data are statistical only. The lines in the same color-code represent the PWA results for the corresponding data sets. The line widths represent the error bands

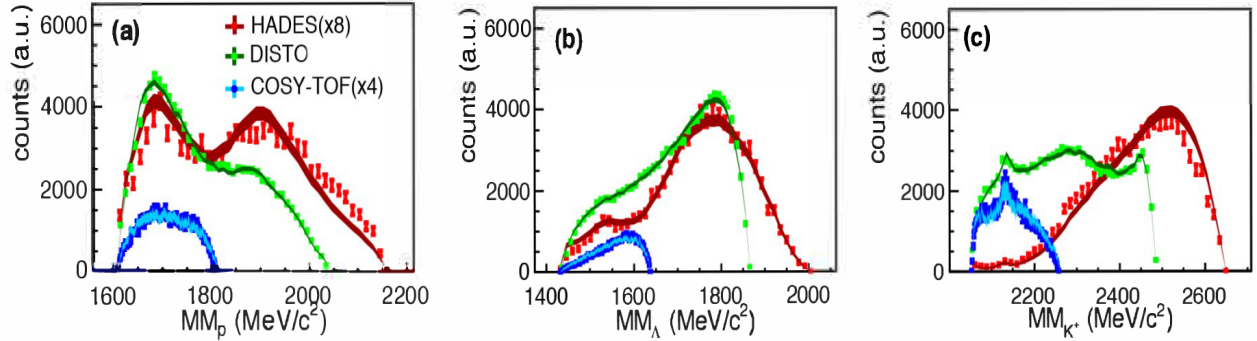


FIG. 1. (Color online). Missing mass distributions (MM) for the three different particles of the final state (p , Λ , K^+) are shown. The experimental data within the geometrical acceptance are from COSY-TOF at 2.16 GeV (blue symbols), DISTO at 2.85 GeV (green symbols) and HADES at 3.5 GeV (red symbols) samples. The colored lines in the same color-code represent the PWA results (see text for details).

of the global PWA fit expressed as the standard deviation of the five best PWA solutions. Figure 2 shows the angular distributions of the three particles measured in the final state for different reference systems for the same data samples discussed in Figure 1. A similar quality is obtained for the description of the kinematic variables of other data samples.

The output of each PWA solution provides the strength of the individual waves with respect to the total measured yield. The resulting relative contributions of the resonant and non-resonant waves can be translated into cross sections for the $K\Lambda$ decay channel multiplying the relative yield by the total production cross section for the $pK^+\Lambda$ final state.

The total $pK^+\Lambda$ cross section for the different data sets was evaluated employing a phase space fit of the existing measurements of the $pK^+\Lambda$ channel as a function of the excess energies [13, 25, 38–40]. The error associated to the $pK^+\Lambda$ cross section of each data sample is extracted from the fit. A detailed description of the extraction of the $pK^+\Lambda$ cross sections can be found in [41].

In Figure 3 the cross section for the different N^* channels decaying into the $K\Lambda$ final state is plotted versus its excess energy calculated as the center of mass energy of the p - p colliding system minus the sum of the proton and N^* masses ($\sqrt{s} - M_{p,N^*}$). The standard deviation of the five best solutions is shown by the black vertical error bars, the green bands show the error originating from the cross section normalization. The non-vanishing cross section below the respective thresholds is due to the large width of all the considered resonances (see Table II). The relative contribution of the non-resonant amplitude decreases from 37% for 2.14 GeV to 10% for 3.5 GeV, so that most of the yield stems from N^* resonances for all the measured energies. The dominant contribution from the N^* resonances is consistent with the results shown in Ref. [13], except for the relative contribution of the

$N^*(1650)$, which is decreasing as a function of the beam energy in [13]. In this work we found an increment of the $N^*(1650)$ similarly to the $N^*(1710)$ and $N^*(1720)$. This difference probably results from neglecting interference in Ref. [13].

The Σ - N cusp contribution varies from 10^{-3} to 10^{-2} with decreasing energy with respect to the N^* and is not shown in Figure 3. The global PWA fit favors the Σ - N cusp contribution of the s - or d -wave state $J^P = 1^+$ with respect to the S -wave $J^P = 0^+$ as shown by the amplitudes in Table IV. The obtained Σ - N cusp yield is slightly different from the findings in Ref. [38] where at a beam energy of 2.28 GeV the contribution of the cusp was found equal to 5% of the total cross section, but neglecting interferences.

Figure 4 shows the cross sections of the different p - p initial states as a function of the $pK^+\Lambda$ excess energy calculated as the center of mass energy of the p - p colliding system minus the sum of the proton Λ and Kaon masses ($\sqrt{s} - M_{p,K^+\Lambda}$). The error bars are associated to the standard deviation of the five best PWA solutions, and the green band refers to the uncertainty of the exclusive $pK^+\Lambda$ production cross section. All extracted cross-sections as a function of the excess energy are summarised in Table IV and Table V.

The non-resonant amplitude included in this PWA is parametrized as a function of the scattering length and effective range for the p - Λ final state interaction. The interference of the non-resonant partial waves with the resonant amplitudes allows us to extract independently the values for S -wave singlet and S -wave triplet partial waves. In Table III the resulting values for the scattering lengths are listed. The values are obtained by averaging the five best PWA solutions. The first error represents the standard deviation of the five fit results. The second one is the PWA fit error obtained by adding quadratically the PWA fit errors from the five solutions. In the

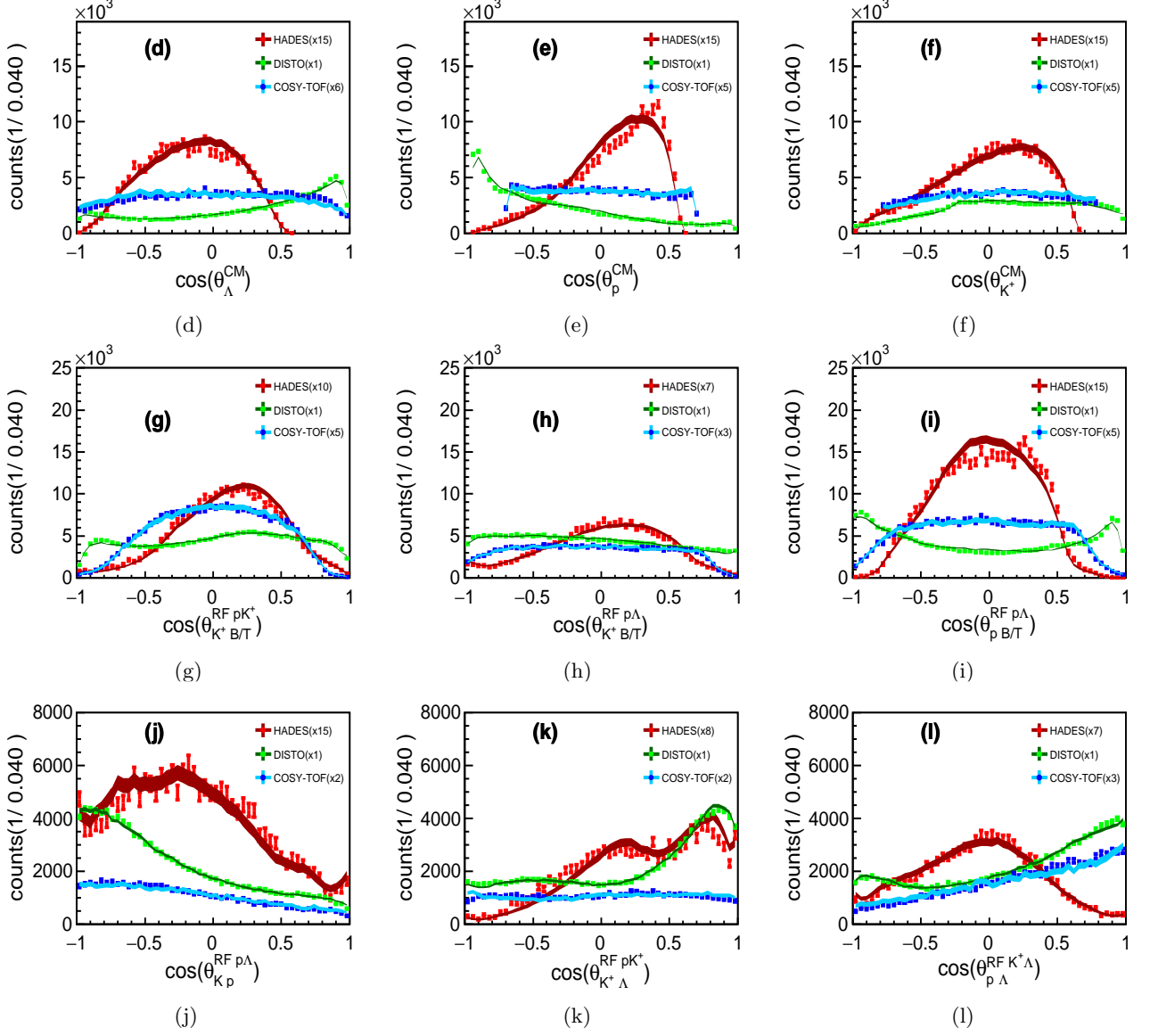


FIG. 2. Angular correlations for the $pK^+\Lambda$ final state. The upper index at the angle indicates the rest frame (RF) in which the angle is displayed. The lower index names the two particles between which the angle is evaluated. CM stands for the center-of-mass system. B and T denote the beam and target vectors, respectively. The observables are: CM distributions ($\cos(\theta_X^{CM})$) of the Λ (d), Proton (e) and Kaon (f); Gottfried-Jackson distributions $\cos(\theta_{KB/T}^{RF pK^+})$ (g), $\cos(\theta_{KB/T}^{RF K\Lambda})$ (h), $\cos(\theta_{pB/T}^{RF p\Lambda})$ (i) and Helicity angle distributions $\cos(\theta_{Kp}^{RF p\Lambda})$ (j), $\cos(\theta_{K\Lambda}^{RF pK^+})$ (k) and $\cos(\theta_{p\Lambda}^{RF K^+\Lambda})$ (l). The experimental data within the geometrical acceptance are from COSY-TOF at 2.16 GeV (blue symbols), DISTO at 2.85 GeV (green symbols) and HADES at 3.5 GeV (red symbols) samples. The colored lines in the same color-code represent the PWA results.

same table also the scattering lengths obtained from p+p reactions with unpolarized [30, 42] and polarized beams [31] and the predictions by recent theoretical calculations [43, 44] are shown.

The results from this PWA are comparable with previously extracted values. Different parametrization, as by means of a Jost function, might modify the extracted scattering parameters. Still, the comparison of

the values that have been extracted within this PWA to other experimental results and theoretical parametrization demonstrate that despite of the very large number of free parameters of this PWA and that all contributions have been treated coherently, a reasonable agreement is achieved.

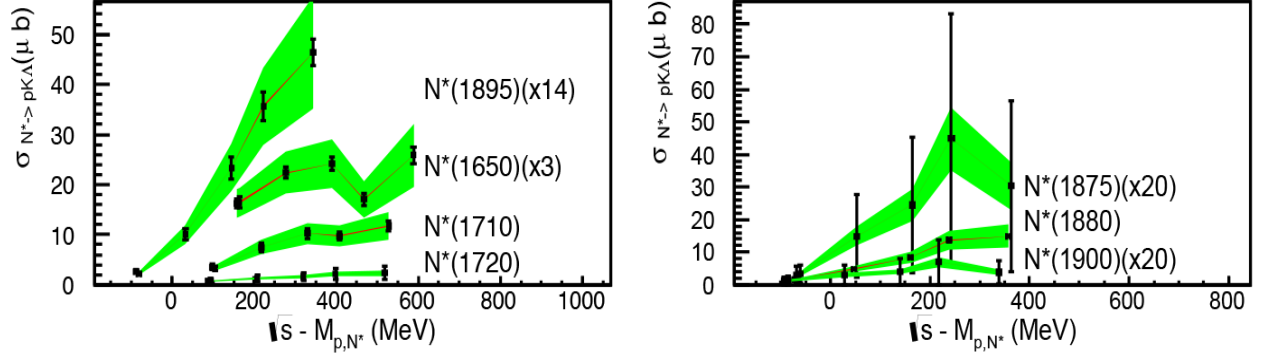


FIG. 3. (Color online). Cross sections of the different N^* resonances decaying into the $pK^+\Lambda$ final state obtained from the combined PWA as a function of the excess energy. The excess energy is calculated as the center of mass energy of the p - p colliding system minus the sum of the proton Λ and Kaon masses ($\sqrt{s} - M_{p,K^+,\Lambda}$). The black bars show the systematic errors originating from the five different PWA solutions and the green bands represent the errors due to the normalization to the total $pK^+\Lambda$ cross section.

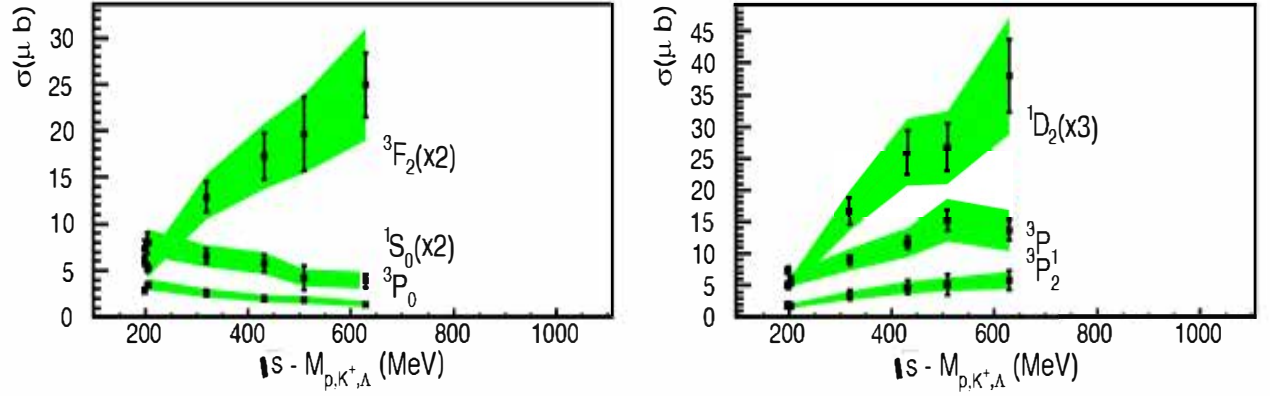


FIG. 4. (Color online). Cross sections of the initial state waves as a function of the excess energy for the $pK^+\Lambda$ final state. The excess energy is calculated as the center of mass energy of the p - p colliding system minus the sum of the proton and N^* masses ($\sqrt{s} - M_{p,N^*}$). The error bars correspond to the standard deviation among the five best PWA solutions and the green band refers to the normalization to the total $pK^+\Lambda$ production cross section.

SUMMARY

We have applied a combined PWA to seven different data sets measuring the reaction $p+p \rightarrow p+K^++\Lambda$ for kinetic energies between 2.14 and 3.5 GeV and determined for the first time the production amplitude of the resonances: $N^*(1650)1/2^-$, $N^*(1710)1/2^+$, $N^*(1720)3/2^+$, $N^*(1875)3/2^-$, $N^*(1880)1/2^+$, $N^*(1895)1/2^-$ and $N^*(1900)3/2^+$ and initial state partial wave as a function of the excess energy. The contribution of the resonances has been found to be dominant with respect to the direct production of the $pK^+\Lambda$ final state especially for the highest kinetic energy of 3.5 GeV where 90% of the yield is associated to N^* . This shows not only that the resonant production is dominating

this energy regime of hadron-hadron collisions, but also provides a quantitative understanding for the first time of the interference effects on the N^* excitation function. The Σ - N cusp was also included in the PWA but its contribution is found to vary between 10^{-3} to 10^{-2} with decreasing energy. Hence it does not influence the obtained results for the N^* and non resonant amplitudes. The p - Λ scattering lengths have also been extracted from this combined PWA and found to be consistent with previous measurements. Higher precision should be achieved with a dedicated analysis of the data at the lowest energies of the here presented data samples. A natural improvement of the results presented in this work will be achieved by including two additional data sets measured by the COSY-TOF collaboration at 2.7 and 2.95 GeV [31, 45].

TABLE III. Scattering lengths extracted from the combined PWA fit and reference values from previous measurements [30, 31, 42] and theoretical calculations [43, 44] (see text for details).

Source	1S_0 $a_{\Lambda-p}$ [fm]	3S_1 $a_{\Lambda-p}$ [fm]
This work	$-1.43 \pm 0.36 \pm 0.09$	$-1.88 \pm 0.38 \pm 0.10$
[30]	$-1.8^{+2.3}_{-4.2}$	$-1.6^{+1.1}_{-0.8}$
[42]	$-2.43^{+0.16}_{-0.25}$	$-1.56^{+0.19}_{-0.22}$
[31]	-	$-2.55^{+0.72}_{-1.39} \pm 0.6 \pm 0.3$
χ EFT LO [43]	-1.91	-1.23
χ EFT NLO [43]	-2.91	-1.54
ESC08 [44]	-2.7	-1.65

ACKNOWLEDGEMENTS

The authors acknowledge the support by funding the following funding agencies: DFG, Grant FA 898/2-1 and NCN 2016/23/P/ST2/04066 POLONEZ.

* robert.muenzer@cern.ch

† laura.fabbietti@ph.tum.de

- [1] J. Schaffner-Bielich, Nucl. Phys. **A804**, 309 (2008), arXiv:0801.3791 [astro-ph].
- [2] D. Chatterjee and I. Vidaa, Eur. Phys. J. **A52**, 29 (2016), arXiv:1510.06306 [nucl-th].
- [3] D. Lonardoni, A. Lovato, S. Gandolfi, and F. Pederiva, Phys. Rev. Lett. **114**, 092301 (2015), arXiv:1407.4448 [nucl-th].
- [4] P. Demorest, T. Pennucci, S. Ransom, M. Roberts, and J. Hessels, Nature **467**, 1081 (2010), arXiv:1010.5788 [astro-ph.HE].
- [5] J. Antoniadis et al., Science **340**, 6131 (2013), arXiv:1304.6875 [astro-ph.HE].
- [6] V. P. Andreev et al., Phys. Rev. **C50**, 15 (1994).
- [7] V. Sarantsev et al., Eur. Phys. J. **A21**, 303 (2004).
- [8] G. Agakishiev et al., Phys. Lett. **B750**, 184 (2015).
- [9] L. Fabbietti et al., Nucl. Phys. **A914**, 60 (2013).
- [10] G. Agakishiev et al., Phys. Rev. **C87**, 025201 (2013).
- [11] G. Agakishiev et al., Phys. Rev. **C85**, 035203 (2012).
- [12] G. Agakishiev et al., Phys. Rev. **C90**, 015202 (2014).
- [13] S. Abd El-Samad et al., Phys. Lett. **B688**, 142 (2010).
- [14] G. Agakishiev et al., Eur. Phys. J. **51**, 137 (2015).
- [15] A. V. Anisovich and A. V. Sarantsev, Eur. Phys. J. **A30**, 427 (2006).
- [16] A. V. Anisovich, V. V. Anisovich, E. Klempt, V. A. Nikonov, and A. V. Sarantsev, Eur. Phys. J. **A34**, 129 (2007).
- [17] K. N. Ermakov, V. I. Medvedev, V. A. Nikonov, O. V. Rogachevsky, A. V. Sarantsev, V. V. Sarantsev, and S. G. Sherman, Eur. Phys. J. **A50**, 98 (2014).
- [18] T. Yamazaki and Y. Akaishi, Physics Letters B **535**, 70 (2002).
- [19] T. Yamazaki et al., Phys. Rev. Lett. **104**, 132502 (2010).
- [20] G. Agakishiev et al., Phys. Lett. **B742**, 242 (2015).
- [21] E. Eppe and L. Fabbietti, Phys. Rev. **C92**, 044002 (2015).
- [22] M. Maggiora et al., Nucl. Phys. **A835**, 43 (2010).
- [23] M. Maggiora, Nucl. Phys. **A691**, 329 (2001).
- [24] F. Balestra et al., Phys. Rev. Lett. **83**, 1534 (1999).
- [25] M. Abdel-Bary et al., Eur. Phys. J. **A46**, 27 (2010).
- [26] R. Münzer, Dissertation, TU München (2014).
- [27] M. Röder et al., Eur. Phys. J. **A49**, 157 (2013).
- [28] B. Sechi-Zorn, B. Kehoe, J. Twitty, and R. A. Burnstein, Phys. Rev. **175**, 1735 (1968).
- [29] F. Eisele, H. Filthuth, W. Föhlisch, V. Hepp, and G. Zech, Phys. Lett. **B37**, 204 (1971).
- [30] G. Alexander et al., Phys. Rev. **173**, 1452 (1968).
- [31] F. Hauenstein et al. (COSY-TOF), Phys. Rev. **C95**, 034001 (2017), arXiv:1607.04783 [nucl-ex].
- [32] J. Adamczewski-Musch et al., Phys. Rev. C **94** (2016).
- [33] C. Patrignani et al. (Particle Data Group), Chin. Phys. **C40**, 100001 (2016).
- [34] A. V. Anisovich et al., Eur. Phys. J. **A48**, 15 (2012).
- [35] K. Ermakov, V. Medvedev, V. Nikonov, O. Rogachevsky, A. Sarantsev, et al., Eur. Phys. J. **A47**, 159 (2011).
- [36] J. D. Jackson, Nuovo Cim. **34**, 1644 (1964).
- [37] A. Gasparyan, J. Haidenbauer, C. Hanhart, and J. Speth, Phys. Rev. **C69**, 034006 (2004), arXiv:hep-ph/0311116 [hep-ph].
- [38] S. Abdel-Samad et al., Eur. Phys. J. **A49**, 41 (2013).
- [39] S. Abdel-Samad et al., Phys. Lett. **B632**, 27 (2006).
- [40] W. G. M. A. Baldini, V. Flaminio and D. R. O. Morrison, in Landolt-Börnstein, New Series, Subvolume a and b (Springer-Verlag, Heidelberg, 1985) p. 417(a) and 468(b).
- [41] R. Muenzer, Proceedings, 12th International Conference on Hypernucl. JPS Conf. Proc. **17**, 062008 (2017).
- [42] A. Budzanowski et al., Phys. Lett. **B687**, 31 (2010).
- [43] J. Haidenbauer, S. Petschauer, N. Kaiser, U. G. Meissner, A. Nogga, and W. Weise, Nucl. Phys. **A915**, 24 (2013), arXiv:1304.5339 [nucl-th].
- [44] T. A. Rijken, M. M. Nagels, and Y. Yamamoto, Progress of Theoretical Physics Supplement **185**, 14 (2010).
- [45] S. Jowzaee et al. (COSY-TOF), Eur. Phys. J. **A52**, 7 (2016), arXiv:1509.03980 [nucl-ex].

TABLE IV. Production cross sections of the total $pK^+\Lambda$ non-resonant contribution and of the different N^* resonances decaying into the $pK^+\Lambda$ final state obtained from the global PWA as a function of the beam kinetic energy. The cross sections refer to the amplitudes prior to the coherent sum of the latter and hence do not consider interference effects. The N^* cross sections are not corrected for the branching ratio into the $K^+\Lambda$ final states. The first error corresponds to the systematic error due to the five best solutions, the second stems from the cross section normalisations. The systematic error of the PWA fitting procedure is found to be negligible and hence is not shown.

	3.500 GeV	3.100 GeV	2.85 GeV
$pK^+\Lambda$ [μb]	$5.1 \pm 1.0 \pm 1.2$	$6.3 \pm 1.2 \pm 1.4$	$6.5 \pm 1.1 \pm 1.3$
$N^*(1650) \rightarrow pK^+\Lambda$ [μb]	$8.6 \pm 0.6 \pm 2.1$	$5.7 \pm 0.4 \pm 1.2$	$8.1 \pm 0.4 \pm 1.6$
$N^*(1710) \rightarrow pK^+\Lambda$ [μb]	$11.7 \pm 1.0 \pm 2.8$	$9.7 \pm 0.8 \pm 2.1$	$10.2 \pm 1.0 \pm 2.1$
$N^*(1720) \rightarrow pK^+\Lambda$ [μb]	$2.4 \pm 1.3 \pm 0.6$	$2.2 \pm 1.2 \pm 0.5$	$1.6 \pm 0.8 \pm 0.3$
$N^*(1875) \rightarrow pK^+\Lambda$ [μb]	$1.5 \pm 1.3 \pm 0.4$	$2.2 \pm 1.9 \pm 0.5$	$1.2 \pm 1.0 \pm 0.2$
$N^*(1880) \rightarrow pK^+\Lambda$ [μb]	$14.9 \pm 0.2 \pm 3.6$	$13.7 \pm 0.4 \pm 3.0$	$8.4 \pm 0.4 \pm 1.7$
$N^*(1895) \rightarrow pK^+\Lambda$ [μb]	$3.3 \pm 0.2 \pm 0.8$	$2.5 \pm 0.2 \pm 0.6$	$1.7 \pm 0.2 \pm 0.3$
$N^*(1900) \rightarrow pK^+\Lambda$ [μb]	$0.2 \pm 0.2 \pm 0.0$	$0.3 \pm 0.3 \pm 0.1$	$0.2 \pm 0.2 \pm 0.0$
$\Sigma-N(1^+S)$ [μb]	$0.01 \pm 0.02 \pm 0.002$	$0.03 \pm 0.02 \pm 0.007$	$0.12 \pm 0.05 \pm 0.02$
$\Sigma-N(1^+D)$ [μb]	$0.13 \pm 0.02 \pm 0.03$	$0.2 \pm 0.04 \pm 0.05$	$0.5 \pm 0.08 \pm 0.1$
	2.5 GeV	2.157 GeV	2.14 GeV
$pK^+\Lambda$ [μb]	$7.2 \pm 1.1 \pm 1.3$	$7.5 \pm 0.6 \pm 1.3$	$7.1 \pm 0.6 \pm 1.2$
$N^*(1650) \rightarrow pK^+\Lambda$ [μb]	$7.5 \pm 0.4 \pm 1.4$	$5.5 \pm 0.3 \pm 1.0$	$5.4 \pm 0.3 \pm 1.0$
$N^*(1710) \rightarrow pK^+\Lambda$ [μb]	$7.5 \pm 0.9 \pm 1.4$	$3.3 \pm 0.5 \pm 0.6$	$3.5 \pm 0.5 \pm 0.6$
$N^*(1720) \rightarrow pK^+\Lambda$ [μb]	$1.3 \pm 0.7 \pm 0.2$	$0.8 \pm 0.4 \pm 0.1$	$0.7 \pm 0.3 \pm 0.1$
$N^*(1875) \rightarrow pK^+\Lambda$ [μb]	$0.7 \pm 0.6 \pm 0.1$	$0.2 \pm 0.1 \pm 0.0$	$0.2 \pm 0.1 \pm 0.0$
$N^*(1880) \rightarrow pK^+\Lambda$ [μb]	$4.8 \pm 0.3 \pm 0.9$	$1.7 \pm 0.1 \pm 0.3$	$1.5 \pm 0.1 \pm 0.3$
$N^*(1895) \rightarrow pK^+\Lambda$ [μb]	$0.7 \pm 0.1 \pm 0.1$	$0.2 \pm 0.0 \pm 0.0$	$0.2 \pm 0.0 \pm 0.0$
$N^*(1900) \rightarrow pK^+\Lambda$ [μb]	$0.2 \pm 0.2 \pm 0.0$	$0.1 \pm 0.1 \pm 0.0$	$0.1 \pm 0.1 \pm 0.0$
$\Sigma-N(1^+S)$ [μb]	$0.12 \pm 0.04 \pm 0.02$	$0.16 \pm 0.04 \pm 0.03$	$0.13 \pm 0.03 \pm 0.02$
$\Sigma-N(1^+D)$ [μb]	$0.34 \pm 0.07 \pm 0.06$	$0.21 \pm 0.04 \pm 0.04$	$0.17 \pm 0.03 \pm 0.03$

TABLE V. Contributions of the different initial state waves as a function of the beam kinetic energy. The obtained cross sections are normalised to the exclusive $pK^+\Lambda$ cross section. The first error corresponds to the systematic error due to the five best solutions, the second originates from the cross section normalisation. The systematic error of the PWA fitting procedure is found to be negligible and hence is not shown.

	3.5 GeV	3.1 GeV	2.85 GeV	2.5 GeV	2.157 GeV	2.140 GeV
$\sigma_{pK\Lambda}$ [μb]	48.0 \pm 5.8	43.1 \pm 5.3	38.7 \pm 4.8	30.5 \pm 3.9	19.7 \pm 2.7	19.0 \pm 2.6
1S_0 [μb]	2.0 \pm 0.4 \pm 0.5	2.1 \pm 0.6 \pm 0.5	2.9 \pm 0.5 \pm 0.6	3.3 \pm 0.4 \pm 0.6	4.0 \pm 0.6 \pm 0.7	3.7 \pm 0.5 \pm 0.6
1D_2 [μb]	12.7 \pm 1.9 \pm 3.0	8.9 \pm 1.2 \pm 1.9	8.6 \pm 1.2 \pm 1.8	5.6 \pm 0.7 \pm 1.0	1.8 \pm 0.1 \pm 0.3	2.5 \pm 0.2 \pm 0.4
3P_0 [μb]	1.4 \pm 0.2 \pm 0.3	1.8 \pm 0.2 \pm 0.4	2.1 \pm 0.3 \pm 0.4	2.6 \pm 0.3 \pm 0.5	3.5 \pm 0.3 \pm 0.6	2.9 \pm 0.2 \pm 0.5
3P_1 [μb]	13.7 \pm 1.4 \pm 3.3	15.3 \pm 1.6 \pm 3.3	11.8 \pm 0.9 \pm 2.4	9.1 \pm 0.7 \pm 1.7	5.9 \pm 0.6 \pm 1.0	5.1 \pm 0.5 \pm 0.9
3P_2 [μb]	5.8 \pm 1.5 \pm 1.4	5.2 \pm 1.5 \pm 1.1	4.8 \pm 1.1 \pm 1.0	3.5 \pm 0.8 \pm 0.7	1.8 \pm 0.4 \pm 0.3	1.9 \pm 0.4 \pm 0.3
3F_2 [μb]	12.5 \pm 1.7 \pm 3.0	9.8 \pm 2.0 \pm 2.1	8.6 \pm 1.2 \pm 1.8	6.4 \pm 0.8 \pm 1.2	2.7 \pm 0.3 \pm 0.5	3.0 \pm 0.3 \pm 0.5